An inverse 3D lung deformation analysis for medical visualization

Anand P Santhanam
School of Computer Science,
University of Central Florida
anand@odalab.ucf.edu

Mudur Pandurang
Computer Science and Software Engineering,
Concordia University
mudur@cs.concordia.edu

Jannick P Rolland
College of Optics and Photonics
University of Central Florida
jannick@odalab.ucf.edu

Abstract.

Medical simulation and visualization of 3D lung deformations is an effective tool for guiding clinical technicians on clinical maneuvers. Technical advances in clinical imaging have led to the extraction of patient-specific 3D static lung models. However, in order to visualize a human subject's lung deformation at different physical conditions, it is required to animate (or deform) the 3D lung models using a physically-based method. In this paper we discuss an approach for estimating the subject-specific lung's deformation operator that models the physically-based elastic interaction undergone in deforming a human's 3D lung model. The transfer function is estimated from the nodal displacements of the 3D lung models obtained from the 4D Computed Tomography (CT) data of a normal human subject and an estimated amount of force applied. Accuracy of the estimated transfer functions is verified by re-simulating the morphology.

Keywords: Organ deformation, Lung morphology, Inverse problems.

1. Introduction

Medical simulation has facilitated the understanding of complex biological phenomenon through its inherent explanatory power. It is a critical component for planning clinical interventions and analyzing its effect on a human subject. The success of medical simulation is evidenced by the fact that over one third of all medical schools in the United States augment their teaching curricula using patient simulators. Medical simulators, such as the mannequin-based trainer VIRGIL, present combat medics and emergency providers with video-based descriptions of patient symptoms along with step-by-step instructions on clinical procedures that alleviate the patient's condition. Recent advances in clinical imaging technology have led to an effective medical visualization by coupling medical simulations with patient-specific anatomical models and their physically and physiologically realistic organ deformation.[1]

The importance of modeling such organ movements and tracking can be seen in the case of radiation oncology. Radiation oncology procedures aim at exposing the lung tumor of a human patient to radiation that destroys the tumor [2, 3]. The effectiveness of the radiation oncology procedure can be significantly increased when the movement of the tumor and the overall lung can be predicted in real-time. The real-time simulation and visualization capability and the physical accuracy of the proposed deformation would facilitate the

development of a real-time clinical guidance system for radiation oncology

Our focus is on modeling the lung's 3D shape dynamics and visualizing it in real-time using Augmented Reality (AR). The technical challenges of designing and visualizing a medical simulation for lung morphology arise in no small part from its computational complexity. Specifically, in an AR environment the position and orientation of the patient are updated by the tracking sensor every 16 ms. Such update requires deforming and rendering 3D lung models at 30-60 times per second[4]. This subsequently limits the usage of high-resolution 3D lung models for real-time deformation and visualization. A method to overcome this limitation was proposed in [5], in which the 3D lung dynamics caused by the air-flow into the lungs were modeled using Green's Formulation (GF). The lung deformation was pre-computed for an upright orientation and simulated in real-time for the upright position. However a generic deformation kernel was used to model 3D lung deformations.

A key requirement to obtain subject-specific lung deformation is to estimate the elastic properties that control the deformation.[6] Of particular interest is the estimation of subject-specific elastic properties that can then be used to animate 3D lung models according to different physical conditions. The variations in the ventilation rates and physical behavior of human breathing, which demonstrates various physical activities of the human subject, can thus be visualized as organ deformations. Clinical technicians can use such organ deformations to assess the patient's condition and to plan the treatment procedure. Additionally, the prognostic estimations of the changes in the organ deformation caused by clinical maneuvers, such as Thorectomy, can also be performed.

Recent advancements in imaging modalities such as ultrasound and magnetic resonance imaging have led to an image-based estimation of tissue elasticity, which is referred to as elastography.[7] Such methods have been extensively applied to analyze tumors and lesions in soft tissues. The common elastic parameter estimated is Young's modulus (YM) which is the ratio between the stress and strain at any particular node or edge.[8] However, the ultrasound-based elastography is not currently used for extracting 3D lung's elastic parameters, due to the lung's air content. The magnetic resonance imaging based elastography is also not currently used for lungs, due to its non real-time imaging. Thus an inverse deformation analysis of 3D lung dynamics may be an essential tool for obtaining the parameters required for accurate deformation.

In this paper we thus focus on non-invasively estimating the deformation operator (also known as the deformation kernel and the transfer function) of patient's specific 3D lungs, which control the lung deformation. It is done by first associating a physically-based deformation method, discussed in [5], to a 4D CT dataset (a sequence of 3D CT datasets representing lung deformations during a single breath) of a patient in a supine posture and then solving for the deformation operator. Specifically, a breath-hold maneuver was used during the imaging process, which avoided any requirement for motion compensation. A 3D polygonal lung model is extracted from a 3D CT dataset and then used to simulate the deformations. It is to be noted that the term 3D model in the paper refers to 3D polygonal models. A single-compartment approach, as previously adopted in [9], [10], [1], and [11], is used for representing the 3D lung model, in which a 3D lung is considered as a single unit instead of a set of lobes. The deformation method uses a kernel (Green's Function (GF)[12]) with surface-level boundary integrals as previously proposed for 3D lung deformations.[13] The inverse deformation (ID) analysis discussed in this paper involves solving for the kernel, for a known displacement, and applied force on each node. The estimated kernel allows simulating a 3D lung surface model according to the human subject's lung tissue property. Additionally, we also modify the kernel

to simulate breathing variations caused by variations in the diaphragm movement. Future work would involve the inclusion of multi-compartment lobular model and the movement of tracheal bifurcations. Such ID analysis for lung deformations has not been previously done to the best of our knowledge.

The paper is further sub-divided as follows: Section 2 discusses related work in estimating tissue parameters. Section 3 discusses the proposed method of inverse deformation analysis and the subsequent results obtained from a 4D CT dataset. Section 4 concludes the paper with a discussion on the future work that needs to be done as an extension of inverse dynamics.

2. Related work

Inverse dynamics (ID) methods allow the estimation of elastic tissue parameters of a 3D object with its known deformation and applied force.[7] Significant amount of work has been done in these methods for applications ranging from simple animations [14]to complex engineering simulations [15]. The general approach for the ID methods is to associate a mathematical representation such as Green's function, Finite Difference Method (FDM), Finite Element Method (FEM), or thin plate deformation [16] to the 3D model's shape change.[12, 17] The ID methods can be more precisely classified based on whether the estimation is done using an iterative approach or in a single step.

An iterative ID approach has been previously addressed for FEM,[18] and thin plate deformations.[16] An iterative inverse FEM analysis uses the following approach. The deformation of the 3D object is first simulated using an initial estimate for the YM values of every node. The simulated deformation is then compared with the actual deformation and the YM's values are updated accordingly. The above steps are repeated until the difference between the simulated and the actual deformation is minimized. For computational simplicity, the value of YM for the tissue or the organ involved is assumed to be a homogenous.[19] The iterative methods currently used for this minimization step are (i) binary selection,[19] (ii) modified newton-raphson,[20] and (iii) levenberg-Markquadt method[21].

An iterative inverse thin-plate deformation method is implemented as follows.[16] A 3D model is first associated with initial values of constants that represent the elastic property in a thin-plate deformation. The deformation was then simulated and compared with the actual observed deformation. The iterative error-optimization is done using the proportional derivative control method.

The non-iterative ID methods have been addressed for FEM, FDM and GF-based deformations. A non-iterative inverse FEM estimates the elastic properties of soft tissues by simplifying the FEM formulation using modal analysis.[14] In this approach the FEM solution is modeled by replacing the mass damping and stiffness matrices with their eigen vectors. The FEM formulation is simplified into the eigen vectors that together with a control vector defines the displacement. The inverse FEM analysis mainly concentrates on computing the control vector.[14]

A non-iterative inverse FDM approach is proposed to estimate the elastic properties of in-compressible volumetric 3D solids using 2D image data-sets.[22] The FDM representation of the 3D solid is first simplified using a Central difference method. The formulation is then inversed to obtain an estimation of YM. The method is, however, computationally expensive and the error-rate in the estimation increased significantly when the number of nodes was increased.[22]

An inverse GF method was developed to estimate the deformation's kernel (operator) for a known deformation.[23] In this method a test-bed was developed which computes this kernel for a 3D object non-iteratively by applying a pre-computed amount of force on a single node using

a robotic arm and scanning the 3D displacements of all the surface points. This pre-computation based method made it possible to achieve 3D deformations in a physically-accurate manner and at interactive rates.[23]

Although iterative optimization forms a key tool in the estimation of elastic tissue parameters they are observed to have two limitations: (i) they may not correctly estimate heterogenous YM, and (ii) the accuracy in estimation may decrease with increase in 3D model complexity. The inaccuracy in estimating heterogenous YM is caused by the complex elastic interactions that occur in those conditions.[6] For instance, any change in the estimation of YM of a node during iterative optimization will alter the convergence of the estimation to the accurate value for neighboring nodes. Thus the convergence of estimation of the YM of every node remains a Cauchy solution [24], which also leads to an increase in the error rate of the elastic estimation for an increase in 3D model complexity.

3. Proposed method

In this paper we present a method to estimate the deformation kernel, which represents the inter-nodal elastic interaction. The estimated kernel can then be used for deforming lung models at any physical condition as previously shown in [25-28] . Additionally, the YM of every node can be estimated from the deformation kernel for diagnostic purposes.

A schematic description of the components involved in the proposed method is shown in Fig.1. We take as input a sequence of

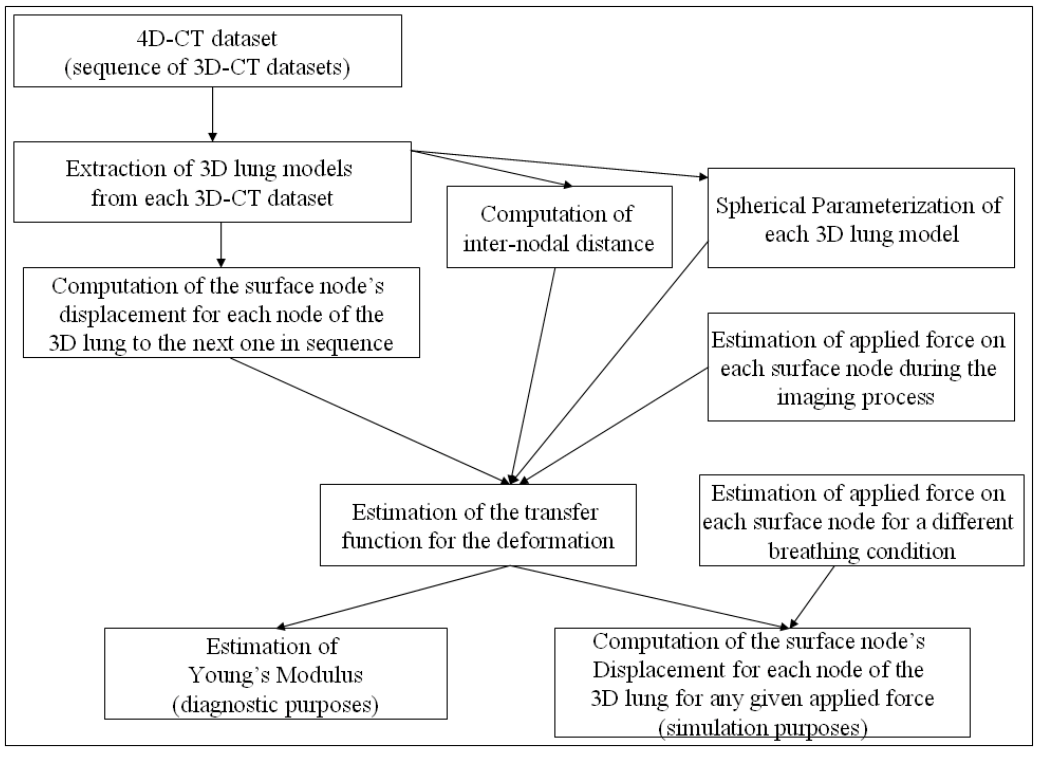

Fig.1. A schematic representation of the proposed method for inverse deformation

4D-CT datsets (sequence of 3D-CT datasets) and an approximate estimate of the airflow during the imaging process. We then extract 3D polygonal models from each of the 3D-CT dataset of the 4D-CT, and compute the inter-nodal distance. Finally, we compute the transfer function that represents the airflow distribution, which is causing the lung deformation. This estimated transfer function can either be used for diagnostic purposes or be used for deforming the 3D lungs under different breathing conditions. From a simulation and visualization perspective, we focus on the latter objective.

This section is further sub-divided as follows: We first discuss the preliminary steps and computation methods in the inverse lung analysis in sub-sections 3.1 to 3.3. We then discuss the relation derived for estimating the transfer function as discussed in sub-section 3.4. This representation allows us to solve for the kernel row for a known applied force and deformation.

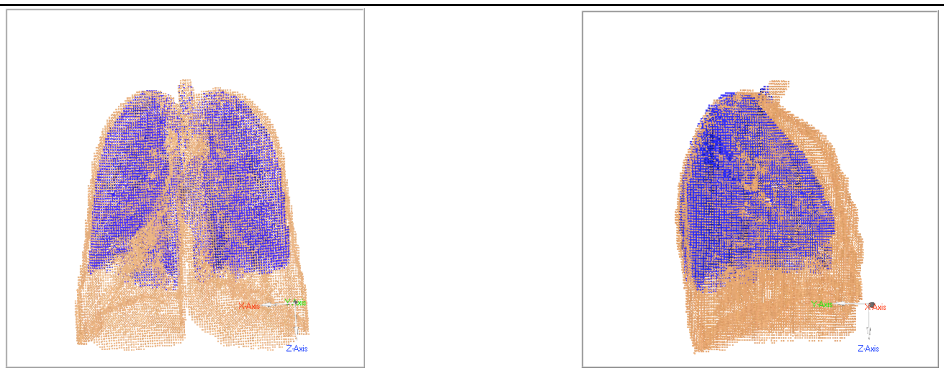

(a) (b)

Fig.2 (a) A front view of human 3D lung model at the start of inhalation (blue) and at the end of inhalation (brown) (b) A side view of human 3D lung model at the start of inhalation (blue) and at the end of inhalation (brown)

3.1 Preliminaries

In this section we first discuss steps involved in the 3D model extraction from 4D-CT datasets. It is followed by a discussion on computing the displacement of surface nodes of the 3D models extracted from each CT dataset. We then briefly discuss the method used for the computation of distance between nodes in a 3D model. Specifically, we discuss a piecewise Euclidean distance computation that allows faster computation of distances along the surface. Finally we briefly discuss the deformation operator used for modeling the lung deformations.

The assumptions based on the theory of lung physiology that are employed for estimating the deformation kernel from the 4D-CT data sets are as follows: First, the clinical data used as input are assumed to have a constant elastic kernel given that the variations in the diaphragm mechanics during the deformation are not considered. Second, the patho-physical tissue behavior is not considered in this paper; this allows us to set

the force applied on each surface node as the vertical pressure gradient.

3.1.1 3D data extraction.

The medical datasets are collected as follows: Four CT scans of a normal patient lying in the supine position. Each scan was taken at a different time point during respiration with the lung volume held at approximately 5%, 40%, 75%, and 100% of the vital capacity as judged by use of a pneumotachometer and high frequency balloon valve which prohibited air flow at the mouth when lung volume reached the desired level on the expiratory limb.[29] The surfaces for the right and left lungs were extracted from each scan and converted into 3D polygon models using the segmentation functions of the Analyze software (developed at the Mayo Clinic).[30] A sequence of four pairs of left and right 3D models were generated from these four scans.

3.2 Nodal displacements computation.

A sequence of four 3D lung models obtained from a normal human lung at 5%, 40%, 75%, and 100% tidal volume at supine position were considered for analysis. Fig.2a and Fig.2b show an illustration of 3D lung models at 5% and at 100% tidal volume. The surface nodes of these 3D models need to be first put in correspondence in order to compute the displacement of nodes. This is done by projecting a ray from a node of the 3D model at 5% tidal volume and performing a ray-triangle intersection analysis of that ray with the lungs at a higher tidal volume. After intersection with triangle of higher tidal volume, the point of the higher tidal volume becomes the corresponding vertex for the vertex at 5% tidal volume The specific direction for each ray is computed using a depth-first searching approach with the constraint that it must allow the displacement's magnitude of every node to be linear with increase in volume as previously observed in [31].

3.3 Piece-wise Euclidean distance computation.

In our work we use a piece-wise Euclidean distance computation instead of a Euclidean distance computation for better estimation of the elastic properties. The piece-wise Euclidean distance between two nodes is computed as follows: For any high-resolution lung model a low-resolution 3D lung model is first created using a commercial software (Geomagic Studio) in such a way that the local curvature details are maintained (this verification is done using Geomagic Studio).

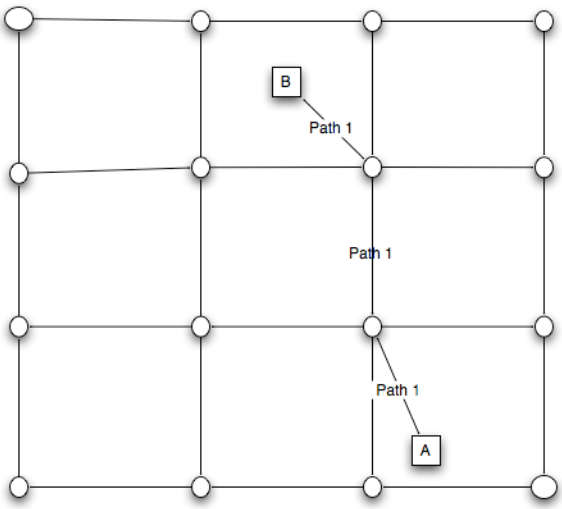

Fig 3. The geodesic path (path 1) between given two nodes A and B of the high-resolution model computed using the low resolution model given as the grid.

Table.1 Discription of parameters used for the introduction of deformation operator

Parameter	***Description***
K(J,I)	*Deformation kernel, which represents the inter-nodal interaction between nodes J and I during a physically-based deformation.*
F(I)	*Force applied on each node I.*
P_I, Q_I	*Structural constants associated with each node I.*
C_I	*Functional constant associated with each node I.*
a(J)	*Alveolar expandability at the region of node I.*
E(J,I)	*Difference between the alveolar expandability of node J and I.*
d(J,I)	*Euclidean distance between two nodes J and I.*
d'(J,I)	*Weighted distance between two nodes J and I.*
Z(J,I)	*Function proportional to d(J,I).*
Z'(J,I)	*Function proportional to d'(J,I).*
A_I,B_I	*Weighted constants used by d'(J,I) to be represented in terms of d(J,I) and e(J,I)*

For computational purposes the low-resolution model is created with 1% of the number of nodes in the high-resolution model. The distance between any two nodes in the low-resolution model is computed using the distance vector method. In this method, a table with the number of rows and columns equal to the total number of nodes is first created and populated using an iterative approach. The creation and population of this table (an iterative procedure) has been extensively discussed in graph theory,[32] and network routing applications. In the case of 3D lung models, the number of iterations to create and populate the distance vector table was observed to be approximately 3. After the creation and population of the table (at equilibrium state) each table element *(x,y)* maintains the two components: (i) the shortest distance between *x* and *y* along the grid and (ii) an immediate neighbor of *x* on the shortest path from *x* to *y*. Finally, every node in the high-resolution model is associated with a set of nodes in the low-resolution model in such a way that the low-resolution nodes surround the high-resolution node. Now in order to compute the distance between any two nodes *(A,B)* in the high-resolution model, we first find the shortest path between any associated nodes of *A* and *B*. We then add the Euclidean distance between *A* and *B* to their respective associated nodes with the shortest path. Fig 3 shows a schematic representation of the path between *A* and *B*.

3.4 Deformation Operator. The general formula of the GF as an operator in discrete space is given as

$$D(I) = \sum_J K(J,I) \times f(J), \tag{1}$$

where *D(I)* is the displacement of the node *I*, *f(J)* is the force applied on node *J,* and *K(J,I)* is the GF operator (deformation kernel), which represents the elastic interaction between nodes taking into account both the inter-nodal distance and elastic properties. The elements of the kernel row represent the normalized weights of the force transferred from one node to another. The elastic interaction in the tissues can be better understood as follows: If we consider the node *I* as the only node on which an external force is applied then there exists a displacement for every other node that is affected by the force applied on *I* through intermediate nodes. This is caused by the transfer of force from one node to another by their elastic interaction. This transfer of forces from node *I* to other nodes is represented as the deformation kernel's row elements, whose row-wise summation is normalized.

Additionally, the elements of the transfer function also represent the YM of the inter-nodal links. The complexity in computing the displacement using the deformation kernel is $O(N^2)$ where N is the total number of nodes in the given 3D lung model.

The general form of the kernel row is described in two different representations. The first one is given as

$$K(J,I) = P_I \cos z(J,I) + Q_I \sin z(J,I) \qquad (2)$$

where $z(J,I)$ is a function that returns a value in the range of zero to 2π. P_I and Q_I are arbitrary constants that take values between zero to 1.[12] The above equation represents the kernel as a continuous trigonometric function discretized by the values of $z(J,I)$. A further mathematical simplification of equation (2) can be given as

$$K(J,I) = C_I \cos z'(J,I), \qquad (3)$$

where C_I is an arbitrary constant and $z'(J,I)$ is a function that returns a value in the range of 0 to $\pi/2$. Equation (3) represents a row of the kernel matrix as a cosine function. The constants P_I and Q_I can be now be written in terms of C_I as

$$P_I = C_I \cos\phi_I \text{ and } Q_I = C_I \sin\phi_I, \qquad (4)$$

Where ϕ_I is a variable parameter that is used later to simulate breathing variations. The second general form of the kernel row is described as a proportionality function of the piecewise Euclidean distance (*d(J,I)*) between *I* and *J*. It can thus be written as

$$K(J,I) = \frac{D_I}{4\pi d(J,I)}, \qquad (5)$$

where *D* is a proportionality constant, which depends on the deformation mechanics of the lungs. Equation (5) has been used for modeling unique cases pertaining to the mechanics. These unique cases discussed by Stakgold present the different values of the proportionality constant.[12] In the case of lungs, the proportionality constant *D* remains unknown.

We now merge the two definitions of the kernel in order to solve for *z'(J,I).* Since both *C* and *D* of equation (3) and (5) act as proportionality constant, the values of cos(z'(J,I)) and $\frac{1}{4\pi d(J,I)}$ can be equated. *z'(J,I)* can now be written as.

$$z'(J,I) = \left[\cos^{-1}\left(\frac{1}{4\pi d(J,I)}\right)\right]. \qquad (6)$$

It can be seen that for higher values of the Euclidean distance between *J* and *I*, the value of *K(J,I)* tends to zero. Additionally, the values of *z'(J,I)* and *d'(J,I)* are proportional. However, in the case of lungs we consider a heterogenous elastic representation in order to account for the regional variations in the alveolar expansion. Thus equation (6) is modified as

$$z'(J,I) = \left[\cos^{-1}\left(\frac{1}{4\pi d'(J,I)}\right)\right], \qquad (7)$$

where *d'(J,I)* is a function that takes into account both the distance and the local elastic properties. It can be seen that for higher values of *d'(J,I)* the value of *K(J,I)* tends to zero. An initial representation for *d'(J,I)* is given as a linear combination of the distance and the elastic interaction.

$$d'(J,I) = A_I d(J,I) + B_J e(J,I), \qquad (8)$$

where A_I and B_I are arbitrary constants. These constants are also referred to as structural constants in this paper, since they both compute the function d'. The function *e(J,I),* which represents the elastic interaction between nodes *J* and *I,* is given as a difference in the alveolar expansion of the region surrounding nodes *J* and *I*. Such a representation is based on the fact that the air flows to the region of least resistance, which in our case is the region of higher alveolar expandability. The regional alveolar expandability is thus an indirect indicator of the YM. The regional alveolar expandability has been previously discussed in [33], [34], and [35]. The function *e* is thus defined as

$$e(J,I) = a(J) - a(I), \qquad (9)$$

where *a(J)* is a function representing an estimated alveolar expandability in the region surrounding node *J*. Equation (9) represents the following fact: the higher the difference between the alveolar expandability, the lower

is the transfer of force. The definition of function e in terms of the alveolar expansion is an essential factor in estimating the kernel for the 3D lungs. It can be seen that the inverse lung deformation problem thus mathematically relates to computing the values of A_I, B_I, and C_I for each node I. Once the C_I for each node is computed, the deformation kernel can be varied by changing the ϕ_I in order to simulate breathing variations.

A method to estimate the values of A_I and B_I using simultaneous equation based representation of equation (7) coupled with approximated kernels, is now discussed. For the 3D lung model extracted from the patient-data, two different estimates of the deformation kernel are first computed. Each deformation kernel is estimated, using only the structural parameters (piecewise Euclidean distance, and regional alveolar expandability). An outline of this method is given in Appendix.A. The second kernel is computed with the following modification: the distance between any two nodes to be twice as that of the distance used in the estimation of first kernel. Now using equation (5) we form two simultaneous equations for each node I, with the unknown being A_I and B_I. The values for the structural constants for each node are thus solved. The values of A_I and B_I are plotted with respect to the Z-axis values of the nodes in the 3D left and right lung models as shown in Fig. 4a, 4b, 4c and 4d respectively. The range of values taken by both A_I and B_I are approximately the same, which leads us to infer that both the inter-nodal distance and local alveolar expandability play an equal role in determining the deformation kernel.

The values for the structural constants for each node are thus solved. The value of C_I can be computed by merging the deformation kernel's expansion given in equation (6) with equation (1). The value of C_I can now be written as

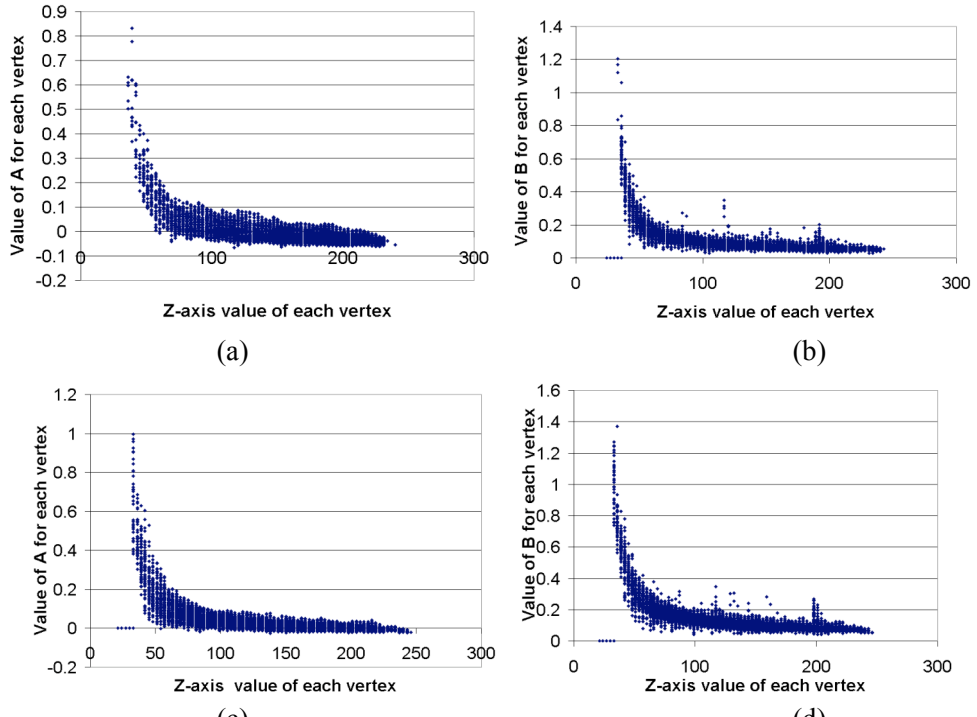

Fig.4. The values of constants A and B are plotted against the Z values of the vertexes for the left lung ((a) and (b)) and right lung ((c) and (d)).

$$C_I = \frac{D[I]}{\sum_{J=0}^{N} f[J] \times \cos(z'(J,I))}. \qquad (10)$$

The values of C_I for left and right lung models are plotted in Fig 5a and 5b respectively. Fig 6a and 6b shows the 3D lungs at the start of the inhalation and at the end of the inhalation. The deformed shape shown in Fig.6b is computed using the deformation kernel estimated from the 4D HRCT model. The total number of nodes on each model is approximately 40000. Once the deformation kernel is estimated, it can be varied for simulating variations in the breathing. Fig.7a and 7b shows two different lung deformations simulated by varying the values of ϕ_I for each node. In each of the images, the deformation lung is shown in red color. For reference, each of the images also includes the undeformed lung in white color. The inclusion of the undeformed lung allows us to show regional changes in the lung shape. Such variations may represent the variations in breathing caused by variations in the diaphragm.

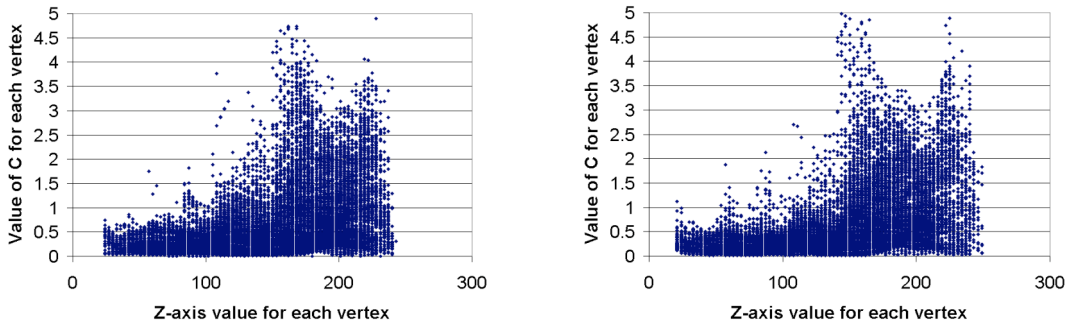

(a) (b)

Fig.5. The values of the C_I are plotted against the Z-axis values of (a) the 3D left lung nodes, and (b) the 3D right lung models.

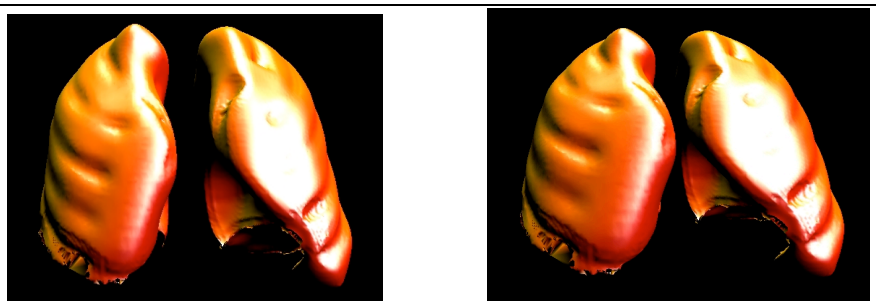

(a) (b)

Fig.6. The 3D lungs (a) at the start of the inhalation and (b) at the end of the inhalation.

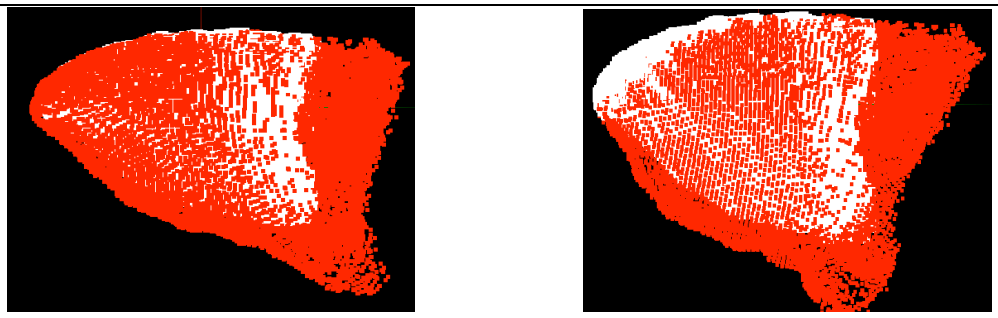

(a) (b)

Fig.7 The 3D deformed lung at the end of inhalation (red color) is shown at two different breathing patterns simulated by varying the values of ϕ_I for (a) and (b). The undeformed lung is shown in white color in both the images.

4. Discussion

A method for inverse lung deformation analysis is discussed in this paper. This method allows obtaining the deformation kernel from 4D-CT images of a human subject data. Such an estimation of kernel allows simulating the 3D lung dynamics of the human subject under different breathing conditions. The inverse problem discussed in this paper solves for these three constants using the deformation kernel. The displacements of the 3D lung nodes were re-constructed from the estimated transfer function with less than 1% RMS error.

The research work discussed in this paper provides extensive scope for analysis in future. These future works would involve (a) validating the 3D lung dynamics simulated at different breathing conditions using invasive methods, (b) modeling the dynamics of a multi-compartmental 3D lung model, (c) accounting for the variations in deformation induced by variations in the diaphragm and rib-cage mechanics, (d) re-constructing the 3D lung dynamic for individual lobes of the 3D lung model, and (e) validating and analyzing the lung dynamics in the presence of a tumor inside lungs.

Appendix A

In this section we briefly explain the method to obtain an estimated deformation kernel for lungs using the inter-nodal distance and alveolar expandability. Every node I of the 3D lung model is first associated with a constant S_I that represents the regional alveolar expandability at that structural location. Additionally, every node I of the 3D lung model is also associated with a value of the force applied on it, which is based on the gravity and is thus based on the orientation of the lung model. We now introduce an initial estimate of the transfer function Te, which is first initialized to 0 and computed as follows.

$$T_e[j \to i] = \left(\frac{S_i}{\sum_{l=0}^{cliqueof(j)} \left(S_l \times \left(\frac{1}{Dist(l,j)}\right)\right)}\right) * \frac{1}{Dist(j,i)} \qquad (A.1)$$

An equilibrium force elastostatic force F applied on each node is estimated using the estimated transfer function and by the following iterative relation

$$F[i] = f[i] \times T_e[i \to i] + \sum_{j=0, j \neq i}^{N} F[j] T_e[j \to i] \qquad (A.2)$$

The final estimate of the transfer function (deformation kernel) T, is computed by the following relation

$$T[j \to i] = \left(\frac{F[j]}{f[j]}\right) \times T_e[j \to i] \qquad (A.3)$$

This deformation kernel is considered as only an estimate since it takes into account the structural properties of a given 3D lung model.

Acknowledgement: This work was funded by the Florida Photonics Center of Excellence and Link fellowship foundation. We thank Dr.Eric

A. Hoffman of University of Iowa for providing 4D CT datasets

Reference

1. Kaye, J.M., F.P.J. Primiano, and D.N. Metaxas, 1998. A Three-dimensional virtual environment for modeling mechanical cardiopulmonary interactions. Medical Image Analysis. **2**(2): 169-195.
2. Murphy, M.J., 2004. Tracking moving organs in real time. Seminars on Radiation Oncology. **14**(1): 91-100.
3. Shirato, H., Y. Seppenwoolde, K. Kitamura, R. Onimura, and S. Shimizu, 2004. Intrafractional tumor motion: lung and liver. Seminars on Radiation Oncology. **14**(1): 10-18.
4. Rolland, J.P., L. Davis, and F. Hamza-Lup, 2003. Development of a training tool for endotracheal intubation: Distributed Augmented Reality. Medicine Meets Virtual Reality (MMVR). **11**: 288-294.
5. Santhanam, A., C. Fidopiastis, F. Hamza-Lup, J.P. Rolland, and C. Imielinska. 2004. Physically-based deformation of high-resolution 3D lung models for augmented Reality based medical visualization. in *Medical Image Computing and Computer Aided Intervention, AMI-ARCS*. Rennes,St-Malo: Lecture Notes on Computer Science.21-32.
6. Metaxas, D., 1997 Physics-based Deformable Models. Philadelphia,PA: Kluwer Academic Publisers.
7. Wilson, L.S., D.E. Robinson, and M.J. Dadd, 2000. Elastography-the movement begins. Physics for Medicine and Biology. **45**.
8. Barber, J.R., 1992 Elasticity. Solid Mechanics and its applications, ed. G.M.L. gladwell. Waterloo,Canada: Kluwer Academic publisher.
9. Promayon, E., P. Baconnier, and C. Puech, 1997. Physically-based model for simulating the human trunk respiration movements. Proceedings of International Joint Conference in CVRMED and MRCAS. **1205**: 121-129.
10. Decarlo, D., J. Kaye, D. Metaxas, and J.R. Clarke. 1995. Integrating Anatomy and Physiology for behavior modeling. in *MMVR*.
11. Segars, W.P., 2002.Development of a new dynamic NURBS-based cardiac-torso (NCAT) phantom. University of North Carolina: Chapel-hill.
12. Stakgold, I., 1979 Green's functions and boundary value problems. Mathematical physics. Wiley Interscience.
13. Santhanam, A., S. Pattanaik, J.P. Rolland, and C. Imielinska. 2003. Physiologically-based real-time 3D lung visualization. in *IEEE Pacific Graphics*. Canmore,Canada: IEEE.
14. Pentland, A. and B. Horowitz, 1991. Recovery of Nonrigid motion and structure. IEEE Transactions on nuclear science. **13**(7).
15. Bukhgeim, A.L., 2000 Introduction to the theory of Inverse Problems. Inverse and Ill-Posed Problems Series. Utrecht: VSP.
16. Metaxas, D.N., 2002. Elastically Adaptive Deformable Models. IEEE Transactions on Pattern Recognition. **24**(10).
17. White.R.E, 1991 An Introduction to Finite Element Methods. Raleigh,NC: John Wiley and Sons.

18. Oberai, A., N. Gokhale, and G.R. Feijoo, 2003. Solution of inverse problems in elasticity imaging using the adjoint method. Institute of Physics publishing.
19. Doyley, M.M., P.M. Meaney, and J.C. Bamber, 2000. Evaluation of an iterative reconstruction method for quantitative elastography. Physics for Medicine and Biology. **45**(152).
20. Fu, D., S.F. Levinson, S.M. Gracewski, and K.J. Parker, 2000. Non-invasive quantitative reconstruction of tissue elasticity using an iterative forward approach. Physics for Medicine and Biology. **45**.
21. Chen, E., W. Naovakofski, K. Jenkins, and W. O'brien, 1996. Young's modulus measurement of soft tissues with application to elasticity imaging. IEEE Transactions on ultrasonics, ferroelectrics and frequency control. **43**(1): 191-194.
22. Raghavan, K.R. and A.E. Yagle, 1994. Forward and Inverse Problems in elasticity imaging and soft tissues. IEEE Transactions on nuclear science. **41**(4).
23. James, D.L. and G.K. Pai, 1999. ARTDefo:Accurate Real-Time Deformable Objects. Annual Conference on Computer Graphics and Interactive Techniques 1999. **33**: 65-72.
24. Reddy, D., 1998 Introductory functional analysis with applications to boundary value problems and finite systems. Texts in Applied Mathematics. New York: Springer Verlag.
25. Santhanam, A., C. Fidopiastis, J.P. Rolland, and P. Davenport. 2006. Real-time simulation of pneumothorax-influenced 3D lung deformations. in *Medicine Meets Virtual Reality*. San Diego CA.
26. Santhanam, A., P. Davenport, C. Fidopiastis, and J.P. Rolland, 2006. A second order differential relation for the pressure-volume relationship of lungs (Submitted). Journal of Applied Physiology.
27. Santhanam, A. and J.P. Rolland, 2006. Simulating 3D lung dynamics in a programmable graphics processing unit. IEEE Transactions on Information Technology and Biomedicine.
28. Santhanam, A., C. Fidopiastis, K. Langen, S. Meeks, P. Davenport, and J.P. Rolland, 2006. Real-time visualization of subject specific lung dynamics. IEEE Computer-based Medical Systems.
29. Tran, B.Q., J.K. Tajik, R.A. Chiplunkar, and E.A. Hoffman, 1996. Lung volume control for quantitative X-ray CT. Journal of Bio-medical Engineering. **24**(s-66).
30. Mayo-Clinic, 2003. Analyze.
31. Fan, L., C.-W. Chen, E.A. Hoffman, and J.M. Reinhardt. 2001. Evaluation and application of 3D lung warping and registration model using HRCT images. in *Proc. SPIE Conf. Medical Imaging*. San Diego,CA.234-243.
32. Baase and Sara, 1988 Computer Algorithms: introduction to design and analysis. Addison-Wesley series in computer science. Addison-Wesley Publications.
33. Calverley, P.M.A., 1995 Chronic Obstructuve Pulmonary Disease, ed. P.M.A. Calverley and N. Pride. London: Chapman and Hall Medical.
34. Jardins, T.D., 1998 Cardiopulmonary anatomy and physiology. Essentials of Respiratory care. Champaign,Illinois: Delmar Publishers.
35. West, J.B., 1995 Respiratory physiology, the essentials. Philadelphia,USA: Lippincott Williams and Wilkins.